Efficient Photocatalyst for the Degradation of Cationic and Anionic Dyes Prepared via Modification of Carbonized Mesoporous TiO_2 by Encapsulation of Carbon Dots

Samaneh Farjadfar [a], Mehran Ghiaci [a,*], Sergei A. Kulinch [b,c], Wilfried Wunderlich [d]

[a] *Department of Chemistry, Isfahan University of Technology, Isfahan, 8415683111, Iran*

[b] *Tokai University, Department of Mechanical Engineering, Hiratsuka, Kanagawa, 259-1292, Japan*

[c] *Far Eastern Federal University, Vladivostok, Russia*

[d] *Tokai University, Department of Material Science, Hiratsuka, Kanagawa 259-1292, Japan*

* *Corresponding author: Email address: mghiaci@iut.ac.ir (Mehran Ghiaci); Tel: +983133913254*

Abstract:

The present work reports on a low-cost synthesis of new nanocomposites consisting of carbon dots (CDs) trapped in a matrix of titanium dioxide. The CDs were prepared directly from polyethylene glycol without any further purification and then trapped in a carbonized mesoporous crystalline TiO_2 (CDs@C-m-TiO_2). The as-prepared photocatalysts were characterized by XRD, FT-IR, FESEM, ~~STEM~~ ?, XPS, PL, DRS, TGA, N_2 adsorption-desorption, and Zeta potential techniques, after which their performance was investigated through degradation of both cationic and anionic organic contaminants. The optimized catalyst showed excellent photocatalytic activity for degradation of methylene blue, rhodamine B, and methyl orange, demonstrating higher efficiency than reference specimens, such as calcined-m-TiO_2, Carbonized-m-TiO_2 or P25 under visible light irradiation. Its efficiency in decaying cationic dyes was found to be better under alkali conditions, while anionic dyes were better destroyed under acidic conditions. Thermogravimetric analysis and consecutive batch runs also displayed both thermal and chemical stability of the prepared CDs@C-m-TiO_2 materials. The results of scavenging tests indicated that the main active sites in the photo-degradation of dyes were holes (h+) generated upon photoexcitation of titanium dioxide. The excellent performance of photocatalysts achieved in this study provides an important step toward the rational design of highly active photocatalysts.

Keywords: photocatalysis; carbon dots; carbonized mesoporous TiO_2; organic dyes.

1. Introduction

The global development of chemical and electronic industries has led to numerous ecological problems [1]. Applying efficient techniques to eliminate organic pollutants from wastewater is considered as one of the most serious challenges in the environmental chemistry. In this respect, photocatalysis has shown a great potential in tackling environmental pollution through the photo-degradation of pollutants [2-7]. Because of their properties, such as thermal stability, low-cost, and non-toxicity, titania based composites have attracted great interest in environmental research communities [8-14]. However, some essential shortcomings of titania such as its bandgap energy (3.2 eV), which is too large for visible light, are known to restrict its industrial applications [14,15]. Therefore, enhancing the light absorption efficiency and increasing the life-time of its photo-generated electron-hole pairs seem to be essential for the efficient degradation of organic dyes by titania based materials [16-18]. A great deal of strategies was developed to modify TiO_2 and improve its photocatalytic efficiency. In this regard, Tang *et al*. synthesized composites containing TiO_2 and high-performance carbon dots (CDs) [19]. Du and co-authors reported on a new hierarchical nanostructure of Ag_3PO_4/TiO_2 [20]. A hybrid of $CdSe/TiO_2$ was used by Yun *et al*. to investigate the nanocrystal size-dependent efficiency of quantum dot sensitized solar cells [21]. Le and coworkers used Rhodamine B dye to sensitize Co-doped TiO_2 material for photocatalytic splitting of water under visible light [22]. Choi *et al*. deposited noble metal Ag on TiO_2 to enhance the photocatalytic hydrogen production on hybrid Ag/TiO_2 in presence of thiocyanate [23]. Lia *et al*. doped mesoporous TiO_2 with tungsten and manganese using SBA-15 as a rigid template, and investigated its photocatalytic activity in degradation of MB [24]. Chen *et al*. hybridized TiO_2 with N-doped carbon to improve its visible-light catalytic activity [25]. The electron-hole pairs could react with O_2 and H_2O and create superoxide anion and hydroxide radicals, thereby increasing the ability of the system to decay numerous industrial organic pollutants.

In recent years, carbonaceous materials such as carbon fibers [26], activated carbon [27], carbon nanotubes [28], and graphene [29] have been applied for enhancing efficiency of TiO_2 as a photocatalyst [30]. As one of carbon-based nanomaterials, CDs received noticeable attention because of their unique properties, such as good biocompatibility, low toxicity, high aqueous solubility, chemical inertness, and easy functionalization [31]. Moreover, they demonstrate very attractive photoelectrical properties, including electron acceptance to inhibit charge recombination, up-conversion, down-conversion photoluminescence (PL), and broad light absorption [32-37]. The surface functional groups of CDs are used as adsorption sites for capturing contaminations [38]. Therefore, photocatalytic composites of CDs/TiO_2 are also prepared to improve the photocatalytic activity of TiO_2. In this regard, Zeng *et al* [39] reported that

CDs, in combination with TiO_2, could improve the production of hydrogen peroxide needed for photocatalytic wastewater treatments. Na and co-workers [40] have used CDs-TiO_2 composite nanosheets for photo-reduction of chromium (VI) under visible light irradiation. Liu *et al.* [41] also used CDs in combination with TiO_2 nanotubes for photo-reduction of Cr(VI) to Cr(III), while Bian and co-workers [42] modified mesoporous TiO_2 by CDs to apply them as photocatalysts for photo-reduction of Cr(VI) to Cr(III). Clearly, the fraction of CDs in a heterojunction can be a critical factor for the photocatalytic performance of prepared photocatalysts.

Keeping these ideas in mind, in this study we focused on three issues. First, we improved the connection between CDs and TiO_2 nanomaterial. Next, we trapped the CDs into the matrix of carbonized mesoporous TiO_2, which was expected to increase the photocatalyst's lifetime. Then, we aimed at developing a photocatalyst that can decompose both cationic and anionic dyes, which should be of great interest economically and industrially. Finally, we changed the concentration of trapped CDs in the matrix of the carbonize-mTiO_2, to find the optimum concentration of CDs in the photocatalyst. As the first step, CDs were prepared from PEG 400 as precursor, and then, they were successfully trapped in a TiO_2 matrix which was prepared as a porous inorganic support generated via the in-situ hydrolysis of titanium (IV) isopropoxide in presence of CDs. The morphology, phase structure, chemical composition, and optical properties of as-prepared CDs@C-mTiO_2 catalysts were characterized by different techniques such as XRD, FT-IR, FESEM, STEM, XPS, PL, DRS, TGA, N_2 adsorption-desorption, and Zeta potential. Then, the synthesized photocatalysts were applied for photo-degradation of organic dyes, showing superior performance in comparison with P25, calcined-mTiO_2 and C-mTiO_2 used as references. Finally, the possible role of CDs, their optimum concentration and the mechanism of photo-degradation were explained based on the experimental data.

2. Experimental section

2.1 Chemicals and materials

Titanium (IV) isopropoxide ($Ti[OCH(CH_3)_2]_4$, 97%) and PEG-400 were obtained from Sigma Aldrich Co. and commercial TiO_2 (P25) was purchased from Degussa (Germany). Organic dyes (methylene blue, rhodamin B, methyl orange), ethylenediaminetetraacetic acid (EDTA), isopropyl alcohol, p-benzoquinone, and absolute ethanol were purchased and used without any further purification. Deionized water was used in all experiments as solvent. Acetonitrile (Merck), ammonium acetate (Sigma Aldrich), phosphoric acid 85% (Merck), and ultrapure water were used for HPLC analysis.

2.2 Synthesis of C-mTiO_2 and CDs@C-mTiO_2

Photocatalysts were fabricated using PEG-400 and Ti[O-i-Pro]$_4$ as sources of CDs and TiO_2, respectively. To prepare CDs, PEG-400 (30 mL) was added into a Teflon-lined autoclave (50 mL) and heated at 180 °C for 6 h. After cooling the product with CDs, a measured volume of CDs (1,2,3,4,6, and 8 mL) was dispersed in absolute EtOH (50 mL) and stirred for 1h. Then, titanium isopropoxide (3 mL) was added dropwise to a dispersion of CDs in ethanol in a 100 mL Morton flask and vigorously stirred for 48 h. The precipitates were then separated by centrifuge, washed with DI water (3x 25 mL) and dried (70 °C) for 24 h. Finally, to obtain TiO_2 as anatase phase, the produced powders were pyrolyzed at 450 °C for 4h in an argon atmosphere with heating ramp of 10°C/min. Thereafter, these samples are denoted as CD1- to CD8@C-m-TiO_2. For preparing the mesoporous TiO_2 containing the residual carbon (C-mTiO_2) as a reference without adding any CDs dispersion, solution of titanium isopropoixe in ethanol was hydrolysed, and then the precipitated TiO_2 was pyrolyzed at 450 °C for 4 h in an argon atmosphere with the ramp of 10 °C/min. Finally, mesoporous TiO_2 (m-TiO_2), without any carbon addition, was obtained by calcination of the hydrolyzed titanium isopropoxide at 450°C for 4 h in the air.

In order to synthesize sample CD-P25, 0.8 g of P25 was added into a Teflon-lined autoclave, then 4 mL of PEG 400 was added and severely stirred for 30 min. The prepared mixture was heated at 180 °C for 6 h. The solid substance was separated by centrifuge, washed with DI water, and dried at 70 °C for 24 h.

2.3 Characterization of photocatalysts

The as-prepared photocatalysts were characterized by XRD, FT-IR, FESEM, STEM, XPS, PL, DRS, TGA, N_2 adsorption-desorption, Zeta potential, and DLS techniques**.** The XRD patterns were obtained on a Philips 87 instrument with a Cu anode (40 kV, 30 mA) over an angular range from 10° to 80°. FT-IR spectra were obtained (4000–400 cm^{-1}) on a Jasco 680 plus FT-IR spectrophotometer (KBr pellets). The FESEM analysis, along with EDS, was run using a TESCAN MIRA3 tool. The STEM images were acquired by a field emission microscope HF 2200 TU operated at an accelerating voltage of 200kV. The PL spectra of liquid samples were recorded on a F-4600 fluorescence spectrophotometer (Hitachi, Japan) at room temperature and using a slit of 5 nm. The PL spectra of solid samples were recorded on a Fluorolog3 spectrofluorometer (Horiba Jobin Yvon) with an excitation source having wavelength 320 nm. The TGA analysis was conceded using a STA503-Pro instrument (Germany) under argon flow (scan range: 30-800 °C) under a heating rate of 10 °C/min. The DRS results were obtained with a Jasco V-670 UV–vis (200–900 nm). The BET surface area was measured with a BELSORP MINI II system (Tokyo, Japan) at

−196 °C using N_2 as adsorbent. Pore volume and pore diameter distribution were taken from the desorption isotherms by applying the Barrett-Joyner-Halenda (BJH) model. Zeta potential and size distribution of CDs were measured by a Horiba Zetasizer Nano ZS-100 tool (Japan). MB, RhB, and MO dye degradation process was analyzed by using an Agilent 1260 infinity with a UV-vis diode array detector using RP-C18 column (250 x 4.6 mm). The mobile phase composed of acetonitrile-ultrapure water 60:40 and 50 mM H_3PO_4 to adjust the pH 3.5 for MB (λ_{max} = 664nm) and RhB (λ_{max} = 554nm). The mobile phase for MO (λ_{max} = 464 nm) was acetonitrile-0.01 M ammonium acetate (30: 70). The flow rate was 1 ml min^{-1}. Before injection, samples were filtered with a Teflon syringe (pore diameter of 0.22 microns).

2.4 Photocatalytic measurements

Photocatalytic activity of samples was evaluated through the degradation of aqueous methylene blue (MB), rhodamine B (RhB) and methyl orange (MO) as model dyes. For each run, 30 mg of catalyst was added to 50 mL of aqueous solution containing MB, RhB or MO (10 mg/L each). The mixture was placed in the dark for 30 min to reach adsorption-desorption equilibrium. Photocatalytic reactions were performed under illumination from a 400 W Xenon-HID lamp with a cutoff filter (to get rid of light under 420 nm) placed at a 10 cm distance from the reaction cell. During irradiation, aliquots of 2 mL were taken after certain time intervals and, after separating photocatalyst powder from dye solution by centrifugation at 10,000 rpm, the concentration of dye was measured by means of UV-vis spectroscopy (JASCO V-570). To investigate the ability of the prepared photocatalysts to decay cationic and anionic dyes simultaneously, tests were performed with a solution containing all three dyes with the concentration of 10 ppm each. For this, 40 mg of CD4@C-mTiO_2 was added to 60 mL of solution with three dyes.

To examine the possibility of successive recycling, tests were performed in the same matter, by separating the photocatalyst via centrifugation at 10,000 rpm for 5 min and washing with absolute ethanol, deionized H_2O, and finally dried at 50 °C for 10 h. To determine the influence of pH on degradation of anionic and cationic dyes, experiments were conducted at different pH values, which were adjusted from 2.5 to 9.5 with the help of HCl and NaOH.

The dye degradation efficiency over time was calculated using Eq. (1):

$$\text{Degradation efficiency (\%)} = [(C_0 - C_t)/C_0] \times 100 \quad (1)$$

where C_0 and C are the initial concentration and the concentration of dye after a time period t, respectively. Uncertainty for all HPLC and UV-vis measurement were less than ± 2%.

2.5 Experiments with free radical scavengers

To evaluate the effect of active species during degradation of anionic and cationic dyes, different free radical scavengers were used. More specifically, IPA, Na_2-EDTA and benzoquinone were applied as scavengers of $^{\bullet}OH$ radicals, photogenerated holes (h^+), and $^{\bullet}O_2^-$, respectively. The tests were performed in the same way as described above for experiments with scavenger-free environment.

3. Results and discussion

3.1 XRD analysis

The powder XRD patterns of the P25 sample and the as-prepared nanocomposites with different amounts of CDs are exhibited in Fig. 1. As well seen in Fig.1a, the P25 sample (blue pattern) had its main peaks at 27.5° (110), 36.1° (101) and 54.3° (211), all of which coming from rutile TiO_2 [43]. At the same time, the XRD pattern of the Carbonized-mTiO_2 sample (green pattern) showed its main peaks at 25.5° (101), 38.05° (004), 48.3° (200), 54.84° (105), 62.7° (204), 69.7° (116) and 75.6° (215), which are indexed as facets of anatase TiO_2 [43]. **Clearly the peaks corresponding to rutile were not observed. However the existence of brookite TiO_2 in the XRD pattern of Carbonized-mTiO_2, can be seen from the (121) diffraction which appeared at 2θ = 30.8° [44]. There is no overlapping of this peak with any one from anatase TiO_2. In mixture brookite/anatase, amount of brookite could be estimated from the relative intensity of their peaks, according to the $I_{brookite}^{(121)}/I_{brookite}^{(120)} + I_{anatase}^{(101)}$ ratio [45]. According to this equation the Carbonized-m-TiO_2 contains approximately 9% brookite phase and 91% anatase phase.** The XRD results of calcined m-TiO_2 and C-m-TiO_2 are presented in Fig. S1, demonstrating that both the calcined samples had comparable patterns. This clearly indicates that the remaining carbon could not change the crystallinity of prepared TiO_2. Upon adding different amounts of CDs into the matrix of Carbonized-mTiO_2, as seen in Fig. 1a, the structure of TiO_2 remains unchanged. The average crystallite sizes of graphitic phase in the composites of Carbonized Mesoporous TiO_2 and CDs@C-mTiO_2 were calculated using the Scherer's formula, and both were found to be about 11 nm. This is in agreement with results obtained from SEM and STEM images. No specific diffraction signal from CDs was observed in the all analyzed nanocomposites, implying that the prepared photocatalysts had CDs well dispersed within the matrix of mesocrystalline anatase TiO_2 [46,47].

3.2. FT-IR studies

Figure 1b shows the FTIR spectra of Carbonized-mTiO_2, CDs and those of CDs@C-mTiO_2 composites. The strong and broad peaks seen at 3400 cm^{-1} and 1640 cm^{-1} observed in all samples can be attributed to the O-H stretching of hydroxyl groups belonging to CDs, to surface-adsorbed water and/or TiO_2 matrix. Such hydroxyl groups can play an important role in photocatalytic activity of the prepared

composites [48]. The peak centered around 1630 cm^{-1} can arise from the bending of O-H groups in all the samples. The peak at 593 cm^{-1} corresponds to the O-Ti-O and Ti-O stretching vibrational motions [49]. Finally, the peaks at 1705 cm^{-1} and 1384 cm^{-1} correspond to the stretching vibrations of C=O and C-C bonds, respectively [50]. The intensity of these peaks was found to increase as the amount of CDs added to samples increased.

3.3. STEM, FESEM, EDX and elemental mapping

FESEM images of samples CD6@C-m-TiO_2, Carbonized-m-TiO_2 and CD2@C-m-TiO_2 are presented in Fig.2a, S2a, and S3a, respectively. As can be seen in Fig. 2a, uniform spherical particles with an average diameter below 100 nm were found in the Carbonized-mTiO_2 support. No visible changes in morphology and particle size in different composites incorporating different amounts of CDs were found by means of SEM.

As shown in Figs. 2b, S2b and S3b, the STEM images confirm the spherical morphology of the NPs in the composites newly prepared in this work. At larger magnification, the materials are seen to have particles with an average diameter below 10 nm, which could be beneficial for their catalytic activity. The elemental analysis performed using EDX (Fig.2c) proved the presence of titanium, oxygen and carbon in the catalysts. Meanwhile, uniform distribution of CDs in the NPs of Carbonized-mTiO_2 was verified by EDX mapping (Fig.2d). More detailed information on the other photocatalysts is presented in Figs. S2 (c, d) and S3 (c, d).

3.4. N_2 adsorption-desorption isotherms

The nitrogen adsorption-desorption isotherms and BJH pore size distribution of sample Mesoporous TiO_2 containing carbon, as well as CD2@C-mTiO_2 and CD6@C-mTiO_2 hybrids are demonstrated in Fig. 3a-c, while results of surface analysis are given in Table 1. According to the IUPAC definitions, all isotherms were recognized as type IV, showing a mesoporous structure with H4 and H2 type hysteresis loops [51,52]. Besides, an average pore size of 1.87, 1.87, and 2.4 nm could be attributed to the Carbonized-mTiO_2, and CD2@C-m-TiO_2 and CD6@C-m-TiO_2 nanocomposites, respectively. Compared with Carbonized-mTiO_2 (specific surface area of 152 m^2/g), the surface area of samples CD2@C-mTiO_2 and CD6@C-m-TiO_2 increased to 185 and 194 m^2/g, respectively, which could probably be attributed to irregularities created by formation of Ti-C bonds in the TiO_2 matrix of the samples. Meanwhile, it should be mentioned that the total volume of the CD2@C-m-TiO_2 composite decreased in comparison with Carbonized-mTiO_2, which could be related to the occupation of some space in the matrix of the Carbonized Mesoporous TiO_2 sample by CDs. On the other hand, the CD6@C-m-TiO_2 composite showed an increase in pore volume. It is believed that its mesoporous structure and increased surface area of the prepared

CDs@C-mTiO_2 nanocomposites would be beneficial for photocatalytic performance, facilitating the diffusion of reactants and products to and from their active sites [53].

3.5. Photoluminescence studies

Photoluminescence emission of the as-prepared nanocomposites was used to evaluate recombination rates of charge carriers (electrons and electron holes) [54]. As can be seen in Fig. 4a, the PL emission intensities were in the order of P25 > Carbonized-m-TiO_2 > CD2@C-m-TiO_2 > CD6@ C-m-TiO_2. Thus, sample P25 that demonstrated the most vigorous PL emission, had the highest recombination rates of its charge carriers. Elevation of the amount of CDs in composites, and even presence of graphitic carbon in their TiO_2 matrix, still resulted in decreased emission intensity, which suggests that CDs could be very important in electron capture or in a more effective separation of photogenerated charge carriers [55,56].

To better understand the results, the photon-conversion property of the CDs was evaluated [58,59]. Fig. 4b, displays the photoluminesent (PL) spectra of CDs dispersed in polyethylene glycol solution that excited by different wavelengths. their PL spectra demonstrated a strong emission peak at~450 nm, which was independent of the excitation wavelength. This indicates that the CDs used exhibited uniformly well-defined surface states and single surface functional groups [60].

3.6. UV-vis diffuse reflectance spectroscopy studies (DRS)

The images of the as-prepared photocatalysts exhibited in Fig.5a show that increase in the amount of CDs in the material leads to darker samples that should absorb the visible light more efficiently [57]. The UV-Vis DRS spectra of sample P25, as well as those of the as-prepared photocatalysts are shown in Fig. 5b. In comparison with P25, the Carbonized-mTiO_2 and CDs@C-mTiO_2 exhibited strong absorption in the visible region, and their absorption depends on CD concentration. In addition, the bandgap of each photocatalyst could be usually determined by the Tauc's relation, according to Eq.(2) [61]:

$$ahv = B\,(hv - E_g)^{1/2} \qquad (2)$$

where α is the absorption coefficient, h is the Plank's constant, v is the photon frequency, B is a constant, and E_g is the bandgap of material. The bandgap of sample P25 was estimated to be 2.8 eV, whereas the bandgaps of the Carbonized-mTiO_2, CD2@C-mTiO_2 and CD6@C-mTiO_2 photocatalysts were estimated to be 2.6 eV, 2.4 eV and 2.0 eV, respectively (Fig.5c). The observed reduction of bandgap confirmed that the presence of CDs could enhance the ability of Carbonized-mTiO_2 to absorb the visible light effectively as it added additional orbitals for the absorption of such photons.

3.7 XPS analysis

To have a deeper insight into the nature and bonding states of the prepared photocatalysts, their X-ray photoelectron spectroscopy (XPS) spectra were recorded and analyzed. Survey scan XPS spectra of the samples, as shown in Fig.6a, had signals of titanium (Ti2p), oxygen (O1s) and carbon (C1s), which is in good agreement with EDX spectroscopy. The core level Ti2p spectrum could be deconvoluted into three components corresponding to Ti^{4+} (458.4, 464.0 eV), Ti^{3+} (456.6, 461.8 eV), and Ti-C (454.6, 460.1 eV) species (Fig.6b). Narrow-scan XPS O1s spectra could be deconvoluted into three peaks corresponding to Ti-O (529.8 eV), C-OH (531.1 eV) and C=O (532.7 eV) bonding (Fig.6c). The C1s XPS spectrum, as shown in Fig. 6d, was curve-fitted using four peaks at 281.4, 284.2, 286.4 and 288.7 eV which were assigned to the Ti-C, C=C, C-O and C=O species, respectively [62-65]. It should be noted that the presence of the Ti-C bond in the CD6@C-mTiO_2 nanocomposite indicated that CDs were incorporated into its TiO_2 matrix [65].

3.8 Photocatalytic performance

Methylene blue and rhodamine B (as cationic dyes) and methyl orange (as anionic dye) were tested in this study as representative organic dyes widely used in academia and industry. To reach the adsorption-desorption equilibrium, at first each nanocomposite was stored in the dark with dye solution for 30 min. This permitted the samples to adsorb dye molecules prior to being irradiated with the visible light. It was found that calcined-m-TiO_2 and Carbonized-m-TiO_2 adsorbed more cationic and anionic dyes when compared with sample P25. On the other hand, the ability of tested photocatalysts to absorb MO was found to be enhanced as they were loaded with higher amounts of CDs, while this trend was not observed for MB and RhB. Figures 7a-c show the photocatalytic performance of different photocatalysts as they decayed MB, RhB and MO under visible-light irradiation. It is seen that, in comparison with sample P25, the calcined-m-TiO_2 and Carbonized-m-TiO_2 composites demonstrated much improved efficiency. The Carbonized-m-TiO_2 could decompose 79% of MB, 77% of RhB and 37% of MO in 35 min. Upon incorporating CDs into the Carbonized-m-TiO_2 network, its efficiency in degradation of the dyes reached as high values as 91% (for MB), 92 % (for RhB), and 95% (for MO) after 35 min.

It is worth noting that the activity of the newly prepared photocatalysts was observed to be different for cationic and anionic dyes. In the case of MB and RhB, increase in CD content over a certain level resulted in a decrease of the catalysts' photodegradation efficiency, while the nanocomposite with a low CD content could decay both cationic dyes well. At the same time, the degradation efficiency of the photocatalyst toward MO was found to enhance as the amount of incorporated CDs increased, which might be related to the absorption ability of this specific dye. According to the literature, the anatase phase of

TiO_2 is an n-type semiconductor, and therefore it has excess electrons beneficial for adsorption of cationic dyes [66]. Hence, the increase in the amount of incorporated CDs could decrease the number of excess electrons on Ti atoms through their transfer to CDs, which should improve the adsorption of anionic dyes. Therefore, the nanocomposite with the highest content of CDs (6 mL added) could degrade anionic dyes more efficiently. It is believed that the dye molecule adsorption is one of key factors determining the photocatalytic performance of nanomaterials toward cationic and anionic dyes. Table 2 indicates that under visible-light irradiation, the nanocomposites prepared in this study demonstrated higher degradation efficiency in comparison with their counterparts prepared by other research groups.

The CD4@C-m-TiO_2 photocatalyst was tested for simultaneous degradation of cationic and anionic dyes in one experiment. Figure 7d shows the results of this test for as long as 35 min. Previously, other groups investigated the degradation of MO, RhB, and MB [67-69]. Upon applying light irradiation, they observed new peaks or peak shift in their HPLC chromatogram or UV-vis spectra. The observed changes were interpreted as dye cleavage, accompanied with formation of low molecular organic intermediates [67-69]. **In the present work, when monitoring the HPLC chromatograms and UV-vis spectra taken during degradation MO, RhB, and MB (Fig.8 a-c), we found no new organic molecules formed, as only peaks related to the dyes were observed to decrease gradually. Therefore, it can be concluded that no detectable intermediates or new organic molecules were produced during the degradation processes taking place in this study. It should be mentioned that as the first stage, each dye absorbed on the surface of the photocatalyst, and then the adsorbed dye can be further decomposed under light radiation [70]. Therefore the adsorption of dyes is crucial in ability of the photocatalyst to degrade them. To prove this, the total organic carbon (TOC) of the tested mixture (containing catalyst and dye) was measured before and after the experiment, giving values of 18.1 and 10 mg L^{-1}, respectively. These values are well consistent with the previously demonstrated UV-Vis spectroscopy results. This indicates that the dyes decayed apparently and converting to CO_2 and water, with no other intermediates registered by the instruments used.**

Figure S6 compares degradation performance of samples CD4@C-m-TiO_2 and P25-CD4 toward MB, RhB, and MO. The adsorption process and photocatalytic activity were found to be inefficient for sample P25-CD4, which is why we assume that the major photocatalytic activity is related to the Carbonized-mTiO_2 material. In case of catanionic dyes, CDs could capture photoinduced electrons to inhibit their recombination with holes, whereas in case of anionic dyes, CDs additionally prevent recombination of electrons and holes, also increasing dye absorption on the surface of the Carbonized-mTiO_2. Both these effects, when combined, should increase the overall photocatalytic performance remarkably, implying a synergistic action of CDs and TiO_2, as the CDs alone cannot show good

photocatalytic activity. **Different molecular structure, charge properties of the dyes, and absorption behavior of the dyes and the photocatalyst create different degradation performance.**

3.9 Kinetic studies

To understand better the mechanisms of photocatalytic performance of the novel photocatalysts, their degradation rate constants for each dye were calculated (Figs. 8a, c, e). The kinetic equation describing dye decay was fitted by a pseudo-first-order rate expression, as represented in Eq. (3):

$$\text{Ln } C/C_0 = -kt \quad (3)$$

where C_0 and C are the initial and current concentrations of dye at different reaction times t, and k is the apparent reaction rate constant [58]. The kinetic plots of all the samples are shown in the Supplementary Materials section. The obtained linear curves and linear regression coefficients (R^2 =97 %) demonstrated that the experimental data could be well fitted to a pseudo-first-order kinetic model. The obtained degradation rate constants of the dyes with different photocatalysts are demonstrated in the Figs. 9b, d, f. The degradation rate constants calculated for MB, RhB and MO over the modified photocatalyst were found to be 0.0724, 0.0696 and 0.0605 min^{-1}, respectively, **which is about 9, 4, and 15 times higher than that of ~~sample~~ the commercially available P25 commonly used as reference. Besides, the apparent rate constants for degradation of the dyes by the modified photocatalysts were about 2, 2, and 5 times higher than that of the carbonized-mTiO$_2$ sample.** Therefore, the above observations imply the importance of incorporation of CDs in order to enhance the ability of Carbonized-mTiO$_2$ material to decay both cationic and anionic dyes.

3.10 Effect of pH

As clearly seen in Figs. 10a-c, dye degradation in presence of all as-prepared photocatalysts was considerably affected by medium pH. The results indicated that the CD2@C-mTiO$_2$ nanocomposite decomposed cationic dyes more effectively under alkaline conditions. In more acidic media, its performance in decaying MB and RhB declined. At the same time, in the case of MO, the efficiency of the photocatalysts in acidic media increased. To provide a better explanation, we measured zeta potential of CDs in aqueous solution in the pH range of 2.5-9.5. As seen in Fig. 10d, the zeta potential of CDs was positive under acidic conditions, while it reached negative values at high values of pH. The found trend is well consistent with the degradation efficiency of the dyes, and it can be attributed to the ability of CDs to take electrons from the Carbonized-mTiO$_2$ material. In acidic media, because of their positively charged surface, the CDs can capture electrons better, and this promotes absorption of anionic dyes but facilitates

desorption of cationic dyes. This leads to the observed enhanced activity in decaying anionic and cationic dyes in acidic environment. In contrast, under alkaline pH conditions, cationic dyes were degraded better than their anionic counterparts. Consequently, the importance of evaluating zeta potential should be emphasized, as its knowledge can help understand how the novel CDs@C-m-TiO_2 photocatalysts absorb dyes under different pH conditions.

3.11 Thermal and chemical stability of the photocatalysts

Thermal and chemical stability are very important operational parameters for any catalyst. Therefore, the newly prepared photocatalysts were tested by means of gravimetric analysis (TGA) and in terms of their reusability. As shown in Fig.11a, all of the new photocatalysts demonstrated high thermal stability. A small weight loss observed below 200 °C could be mainly due to evaporation of the adsorbed water [59]. Between 200 °C and 800 °C, a weight loss of 3.5 % could be attributed to phase changes of the mesoporous TiO_2 and removal of water adsorbed during such changes [77,78]. As can be seen in Fig. 11a, the thermal behavior of samples Carbonized-m-TiO_2 and CDs@C-mTiO_2 was similar, showing that CDs remained stable during the tests [40]. The reusability of the CDs@C-m-TiO_2 nanocomposites was determined by the chemical stability of each constituent after dye degradation. For this test, the photocatalysts were separated from reaction mixture after each run by centrifugation, after which washed with ethanol and deionized water. Finally, they were dried at 50 °C before the next recycling test. Figure 11b shows the performance of the optimal photocatalyst for five consecutive runs in presence of MB. It is well seen that the photocatalyst was reused without any changes in its photocatalytic activity even after five runs. Based on these results, the newly developed CDs@C-m-TiO_2 nanocomposites are concluded to have good thermal and chemical stability.

3.12 Mechanistic insights

Experiments with active species. Tests with different scavengers were used to determine the contribution of active species during dye photodegradation by sample CD2@C-mTiO_2. According to the literature, superoxide radicals ($\cdot O_2^-$), holes (h^+) and hydroxyl radicals (·OH) are the three main active species acting in photodegradation reactions. In this study, benzoquinone (BQ), disodium ethylenediaminetetraacetate (Na_2-EDTA), and isopropyl alcohol (IPA) were used to trap $\cdot O_2^-$, h^+ and ·OH species, respectively [79,80]. As shown in Fig. 11c, the photocatalytic activity of sample CD2@gC-m-TiO_2 was significantly affected by different scavengers. Its performance was considerably decreased after addition of Na_2-EDTA as a hole scavenger. Without scavengers, the degradation efficiency of this photocatalyst was ~84% after 30 min, while it dropped to 80, 66 and 35% upon adding BQ, IPA and Na_2-

EDTA, respectively. These results also imply that the holes were the main active species in our experiments, while hydroxyl radical also played a critical role.

Cyclic voltammetry measurements. In order to verify the conduction band (CB) and valence band (VB) of the catalysts, cyclic voltammetry measurements were carried out. The oxidation and reduction peaks are related to electrons and holes injected into the conduction and valence bands. The values of E_{CB} and E_{VB} were calculated by using the following equations [81,82]:

$$E_{CB} = -e\,[4.75 + E_{red}] \quad (4)$$

$$E_{VB} = -e\,[4.75 + E_{ox}] \quad (5)$$

$$E_{NHE} = E_{Ag/AgCl} + 0.197 \quad (6)$$

Cyclic voltammetry results showed a reduction peak at -1.35 eV and an oxidation peak at 1.24 eV for sample Carbonized-mTiO_2 versus the Ag/AgCl electrode. Therefore, the values for E_{CB} and E_{VB} were calculated to be -6.22 and -3.5eV, respectively. Since $E_g = E_{CB} - E_{VB}$, the E_g of sample C-m-TiO_2 was found to be 2.63 eV, which agrees with the value extracted from its Tauc's plot.

Based on the above discussions, CDs incorporated into the nanocomposites play an essential role, significantly enhancing their photocatalytic performance. According to the DRS UV-Vis analysis, CDs can considerably improve the visible-light adsorption of the as-prepared catalysts. Also, based on the photoluminescence spectra, CDs increased the separation rate of the photogenerated electron-hole pairs. The combination of increased adsorption of visible light and more efficient separation of electron-hole pairs could be responsible for the observed enhanced photocatalytic activity. The Scheme in Fig.12 shows the mechanism of photocatalytic reactions based on our results and literature data. **According to this mechanism, the carbonized mesocrystalline titanium dioxide adsorbs visible light, followed by the excitation of electron from valance band (V_B) to the conduction band (C_B), and generating the electron-hole pairs. The incorporated carbon dots immediately capture the produced electrons, thus preventing recombination of photogenerated electron-hole pairs and generated holes in valance band of C-mTiO_2. Finally, the photogenerated holes can result in the formation of hydroxyl radicals responsible for the decay of adsorbed dye molecules.**

4. Conclusions

A novel composite photocatalyst based on carbon dots (CDs) incorporated into Carbonized mesoporous TiO_2 with its porous inorganic matrix was developed in this work. The CDs were prepared from PEG without any additives or further treatment, after which they were coated with Carbonized

mesoporous crystalline TiO_2. The prepared nanocomposites were proved to be photocatalysts with good reusability and stability. Compared with sample P25 used as reference, the newly developed photocatalyst (more specifically, CD- incorporated C-m-TiO_2) showed superior performance with twelve, five and twenty-three times higher degradation rates for MB, RhB and MO, respectively. It was found that CDs could improve the photocatalytic activity of the novel material through: (i) better separation of photogenerated charges, (ii) increasing visible light absorption, (iii) enlarging surface area, and finally (iv) delocalizing electrons and donating more positive surface charge to the mesoporous TiO_2 that wrapped them. Optimal conditions for decay of cationic and anionic pollutants by the novel photocatalyst were also found. While basic pH provided the best conditions for cationic dyes, anionic dyes were better degraded under acidic conditions. Finally, a mechanism based on adsorption–photodegradation was suggested to explain the observed degradation of cationic and anionic pollutants by the novel photocatalyst.

Supporting Information

Additional experimental results are available in the file downloadable under *Supplementary Material*.

Acknowledgments. We are grateful for the financial supports provided by Isfahan University of Technology; technical supports from Tokai University should be appreciated too. The authors also thank Dr. S.M. Hosseini and Dr. S.K. Movahed, both from Isfahan Tech, for their help with experiments and XPS analysis.

References

[1] Z. Carmen, S. Daniela, "Textile organic dyes–characteristics, polluting effects and separation/elimination procedures from industrial effluents–a critical overview," in Organic pollutants ten years after the Stockholm convention-environmental and analytical update, 2012, p. 32373, doi: 10.5772/32373.

[2] L. Yang, Y. Xiao, S. Liu, Y. Li, Q. Cai, S. Luo, G. Zeng, "Photocatalytic reduction of Cr (VI) on WO_3 doped long TiO_2 nanotube arrays in the presence of citric acid," Appl. Catal. B 94 (2010) 142-149, doi: 10.1016/j.apcatb.2009.11.002.

[3] M. Qamar, M. Gondal, Z. Yamani, "Laser-induced efficient reduction of Cr (VI) catalyzed by ZnO nanoparticles," J. Hazard. Mater. 187 (2011) 258-263, doi: 10.1016/j.jhazmat.2011.01.007.

[4] Y. Ku, Y.-H. Huang, Y.-C. Chou, "Preparation and characterization of ZnO/TiO_2 for the photocatalytic reduction of Cr (VI) in aqueous solution," J. Mol. Catal. A 342 (2011) 18-22, doi: 10.1016/j.molcata.2011.04.003.

[5] Q. Wu, J. Zhao, G. Qin, C. Wang, X. Tong, S. Xue, "Photocatalytic reduction of Cr (VI) with TiO_2 film under visible light," Appl. Catal. B 142 (2013) 142-148, doi: 10.1016/j.apcatb.2013.04.056.

[6] Y. C. Zhang, L. Yao, G. Zhang, D. D. Dionysiou, J. Li, X. Du, "One-step hydrothermal synthesis of high-performance visible-light-driven SnS_2/SnO_2 nanoheterojunction photocatalyst for the reduction of aqueous Cr (VI)," Appl. Catal. B 144 (2014) 730-738, doi: 10.1016/j.apcatb.2013.08.006.

[7] F. Zhang, Y. Zhang, C. Zhou, Z. Yang, H. Xue, D. D. Dionysiou, "A new high-efficiency visible-light photocatalyst made of SnS_2 and conjugated derivative of polyvinyl alcohol and its application to Cr (VI) reduction," Chem. Eng. J. 324 (2017) 140-153, doi: 10.1016/j.cej.2017.05.009.

[8] M. Xing, Y. Zhou, C. Dong, L. Cai, L. Zeng, B. Shen, L. Pan, C. Dong, Y.Chai, J.Zhang, and Y.Yin, "Modulation of the reduction potential of TiO_{2-x} by fluorination for efficient and selective CH_4 generation from CO_2 photoreduction," Nano Lett. 18 (2018) 3384-3390, doi: 10.1021/acs.nanolett.8b00197.

[9] S. Feizpoor, A. Habibi-Yangjeh, S. Vadivel, "Novel TiO_2/Ag_2CrO_4 nanocomposites: efficient visible-light-driven photocatalysts with n–n heterojunctions," J. Photochem. Photobiol. A 341 (2017) 57-68, doi: 10.1016/j.jphotochem.2017.03.028.

[10] H. Li, Y. Sun, Z. Y. Yuan, Y. P. Zhu, T. Y. Ma, "Titanium phosphonate based metal-organic frameworks with hierarchical porosity for enhanced photocatalytic hydrogen evolution," Angew. Chem. 130 (2018) 3276-3281, doi: 10.1002/ange.201712925.

[11] X. Guo, Y. Zhu, T. Ma, "Lowering reaction temperature: Electrochemical ammonia synthesis by coupling various electrolytes and catalysts," J. Energy Chem. 26 (2017) 1107-1116, doi: 10.1016/j.jechem.2017.09.012.

[12] H. Ge, L. Cui, Z. Sun, D. Wang, S. Nie, S. Zhu, B. Matthews, G. Wu, X. Song, and T. Ma "Unique $Li_4Ti_5O_{12}$/TiO_2 multilayer arrays with advanced surface lithium storage capability," J. Mater. Chem. A 6 (2018) 22053-22061, doi: 10.1039/C8TA03075H.

[13] Z. Min, X. Wang, Y. Li, J. Jiang, J. Li, D. Qian, and J. Li, "A highly efficient visible-light-responding Cu_2O- TiO_2/g-C_3N_4 photocatalyst for instantaneous discolorations of organic dyes," Mater. Lett. 193 (2017) 18-21, doi: 10.1016/j.matlet.2017.01.083.

[14] Z. Lu, Z. Zhu, D. Wang, Z. Ma, W. Shi, Y. Yan, X. Zhao, H. Dong, L. Yang, and Z. Hua, "Specific oriented recognition of a new stable ICTX@Mfa with retrievability for selective photocatalytic degrading of ciprofloxacin," Catal. Sci. Technol. 6 (2016) 1367-1377, doi: 10.1039/C5CY01324K.

[15] O. Carp, C. L. Huisman, A. Reller, "Photoinduced reactivity of titanium dioxide," Prog. Solid State Chem. 32 (2004) 33-177, doi: 10.1016/j.progsolidstchem.2004.08.001.

[16] T. M. Elmorsi, Y. M. Riyad, Z. H. Mohamed, H. M. Abd El Bary, "Decolorization of mordant red 73 azo dye in water using H_2O_2/UV and photo-Fenton treatment," J. Hazard. Mater. 174 (2010), 352-358. 2010, doi: 10.1016/j.jhazmat.2009.09.057.

[17] Ş. Gül and Ö. Özcan-Yıldırım, "Degradation of reactive red 194 and reactive yellow 145 azo dyes by O_3 and H_2O_2/UV-C processes," Chem. Eng. J. 155 (2009) 684-690, doi: /10.1016/j.cej.2009.08.029.

[18] B. Viswanathan, "Photocatalytic degradation of dyes: An overview," J. Curr. Catal. 7 (2018) 99-121, doi: 10.2174/2211544707666171219161846.

[19] Y. Tang, H. Rong, F. Yu, J. Yong, Z. Xiangcheng, P. Qingjiang, and J. Baojiang, "Carbon quantum dot/mixed crystal TiO 2 composites via a hydrogenation process: an efficient photocatalyst for the hydrogen evolution reaction." RSC Adv .6. 99 (2016) 96803-96808, doi: 0.1039/C6RA17597J

[20]. D, Guangqian. J.Yuan, and C. Zhu, "Hierarchical nanostructures of Ag 3 PO 4 on TiO_2 nanofibers with enhanced photocatalytic activity for the degradation of rhodamine B." J. Mater. Sci. - Mater. Electron. 28. 10 (2017) 7307-7312, doi: 10.1007/s10854-017-6416-6

[21] H.J, Yun. T, Paik. D, Benjamin. E.E, Michael. B. B, Jason. B.M, and Christopher. "Nanocrystal size-dependent efficiency of quantum dot sensitized solar cells in the strongly coupled CdSe nanocrystals/TiO_2 system." ACS Appl. Mater. Interfaces 8. 23 (2016) 14692-14700, doi:10.1021/acsami.6b05552

[22] T.T. Le, A. M. Shaheer, P.M. Dong, L. C. Jang, and Y. O-Bong,"Water splitting on Rhodamine-B dye sensitized Co-doped TiO_2 catalyst under visible light." Appl. Catal., B. 111 (2012) 397-401, doi: 10.1016/j.apcatb.2011.10.023

[23] Y. Choi, K. Hyoung-il, M. Gun-hee, J. Seongwon, and C. Wonyong , "Boosting up the low catalytic activity of silver for H_2 production on Ag/TiO_2 photocatalyst: thiocyanate as a selective modifier." ACS Catal, 6. 2 (2016) 821-828, doi: 10.1021/acscatal.5b02376

[24] S. Liu, G. Enyan, and Y. Longwei,"Tailored visible-light driven anatase TiO 2 photocatalysts based on controllable metal ion doping and ordered mesoporous structure." J. Mater. Chem, 22. 11 (2012) 5031-5041, doi: 10.1039/C2JM15965A

[25] X. Chen, X. Zongli , J. Yan , W. Jing, Z. Yonggang, H. Yuning, Z. Xiwang , and W. Huanting , "Hybridizing TiO_2 with Nitrogen‐Doped Carbon: A New Route to A Highly Visible Light‐Active Photocatalyst." Chem.Sel 2. 4 (2017) 1565-1572, doi: 10.1002/slct.201700017

[26] J. Zhang, Y. Li, L. Li, W. Li, C. Yang, "Dual functional N-doped TiO_2-carbon composite fibers for efficient removal of water pollutants," ACS Sustainable Chem. Eng. 6 (2018) 12893-12905, doi: 10.1021/acssuschemeng.8b02264.

[27] X. Fu, H. Yang, H. Sun, G. Lu, J. Wu, "The multiple roles of ethylenediamine modification at TiO_2/activated carbon in determining adsorption and visible-light-driven photoreduction of aqueous Cr (VI)," J. Alloys Compd. 662 (2016) 165-172, doi: 10.1016/j.jallcom.2015.12.019.

[28] K. Dai, X. Zhang, K. Fan, T. Peng, and B. Wei, "Hydrothermal synthesis of single-walled carbon nanotube–TiO_2 hybrid and its photocatalytic activity," Appl. Surf. Sci. 270 (2013) 238-244, doi: 10.1016/j.apsusc.2013.01.010.

[29] N. N. T. Ton, A. T. N. Dao, K. Kato, T. Ikenaga, D. X. Trinh, T. Taniike, "One-pot synthesis of TiO_2/graphene nanocomposites for excellent visible light photocatalysis based on chemical exfoliation method," Carbon 133 (2018) 109-117, doi: 10.1016/j.carbon.2018.03.025.

[30] X. T. Zheng, A. Ananthanarayanan, K. Q. Luo, P. Chen, "Glowing graphene quantum dots and carbon dots: properties, syntheses, and biological applications," Small 11 (2015) 1620-1636, doi: 10.1002/smll.201402648.

[31] Y. Wang, and H. Aiguo, "Carbon quantum dots: synthesis, properties, and applications." J. Mater. Chem. C. 2 34 (2014) 6921-6939, doi: 10.1039/C4TC00988F.

[32] P. Yang, Z. Jianghong, W. Jian, C. Baoyue, L. Li, and Z. Zhenping, "Light-induced synthesis of photoluminescent carbon nanoparticles for Fe 3+ sensing and photocatalytic hydrogen evolution." J. Mater. Chem. A. 3 (2015) 136-138, doi: 10.1039/c4ta05155f.

[33] S. Y. Lim, W. Shen, Z. Gao, "Carbon quantum dots and their applications," Chem. Soc. Rev. 44 (2015) 362-381, doi: 10.1039/C4CS00269E.

[34] R. Das, R. Bandyopadhyay, P. Pramanik, "Carbon quantum dots from natural resource: A review," Mater. Today Chem. 8 (2018) 96-109, doi: 10.1016/j.mtchem.2018.03.003.

[35] L. Li, G. Wu, G. Yang, J. Peng, J. Zhao, J.-J. Zhu, "Focusing on luminescent graphene quantum dots: current status and future perspectives," Nanoscale 5 (2013) 4015-4039, doi: 10.1039/C3NR33849E.

[36] L. W. Zhang, H. B. Fu, Y. F. Zhu, "Efficient TiO_2 photocatalysts from surface hybridization of TiO_2 particles with graphite-like carbon," Adv. Funct. Mater. 18 (2008) 2180-2189, doi: 10.1002/adfm.200701478.

[37] H. Li, Z. Kang, Y. Liu, S.-T. Lee, "Carbon nanodots: synthesis, properties, and applications," J. Mater. Chem. 22 (2012) 24230-24253, doi: 10.1039/C2JM34690G.

[38] X. Zheng, A. Arundithi, Q. Kathy, and C. Peng, "Glowing graphene quantum dots and carbon dots: properties, syntheses, and biological applications." small 11. 14 (2015) 1620-1636, doi: 10.1002/smll.201402648.

[39] X. Zeng, Z. Wang, Na. Meng, D. McCarthy, A. Deletic, J. Pan, X. Zhang, "Highly dispersed TiO_2 nanocrystals and carbon dots on reduced graphene oxide: Ternary nanocomposites for accelerated photocatalytic water disinfection", Appl. Catal., B 202 (2017) 33-41, doi: 10.1016/j.apcatb.2016.09.014.

[40] Y. Li, Z. Liu, Y. Wu, J. Chen, J. Zhao, F. Jin, and P. Na, "Carbon dots-TiO_2 nanosheets composites for photoreduction of Cr (VI) under sunlight illumination: favorable role of carbon dots," Appl. Catal., B 224 (2018) 508-517, doi: 10.1016/j.apcatb.2017.10.023.

[41] W. Liu, J. Ni, X. yin, "Synergy of photocatalysis and adsorption for simultaneous removal of Cr (VI) and Cr (III) with TiO_2 and titanate nanotubes," Water Res. 53 (2014) 12-25, doi: 10.1016/j.watres.2013.12.043.

[42] Y. Zhang, M. Xu, H. Li, H. Ge, Z. Bian, "The enhanced photoreduction of Cr (VI) to Cr (III) using carbon dots coupled TiO_2 meso crystals", Appl. Catal., B 226 (2018) 213-219, doi: 10.1016/j.apcatb.2017.12.053.

[43] H. Ijadpanah-Saravy, M. Safari, A. Khodadadi-Darban, A. Rezaei, "Synthesis of titanium dioxide nanoparticles for photocatalytic degradation of cyanide in wastewater," Anal. Lett. 47 (2014) 1772-1782, doi: 10.1080/00032719.2014.880170.

[44] Y Wang, Y Li. "Template-free preparation and photocatalytic and photoluminescent properties of Brookite TiO_2 hollow spheres." J. Nanomater 2019 (2019), doi: 10.1155/2019/3605976

[45] L Ji-Guang, I Takamasa, and S Xudong. "Anatase, brookite, and rutile nanocrystals via redox reactions under mild hydrothermal conditions: phase-selective synthesis and physicochemical properties." J. Phys. Chem. C 111, no. 13 (2007), 4969-4976. , doi: 10.1021/jp0673258

[46] P. Ferreira, I. Fonseca, A. Ramos, J. Vital, J. Castanheiro, "Acetylation of glycerol over heteropolyacids supported on activated carbon," Catal. Commun. 12 (2011) 573-576, doi: 10.1016/j.catcom.2010.11.022.

[47] P. Ferreira, I. Fonseca, A. Ramos, J. Vital, J. Castanheiro, "Esterification of glycerol with acetic acid over dodecamolybdophosphoric acid encaged in USY zeolite," Catal. Commun. 10 (2009) 481-484, doi: 10.1016/j.catcom.2008.10.015.

[48] C.-Y. Wu, K.-J. Tu, J.-P. Deng, Y.-S. Lo, C.-H. Wu, "Markedly enhanced surface hydroxyl groups of TiO_2 nanoparticles with superior water-dispersibility for photocatalysis," Materials 10 (2017) 566, doi: 10.3390/ma10050566.

[49] H. Foratirad, H. R. Baharvandi, M. G. Maragheh, "Chemo-rheological behavior of aqueous titanium carbide suspension and evaluation of the gel caster green body properties," Mater. Res. 20 (2017) 175-182, doi: 10.1590/1980-5373-mr-2016-0410.

[50] Y. Guo, D. Wang, X. Liu, X. Wang, W. Liu, W. Qin, "Synthesis and characterization of the nickel@ carbon dots hybrid material and its application in the reduction of Cr (VI)," New J. Chem. 38 (2014) 5861-5867, doi: 10.1039/C4NJ01087F.

[51] P.B. Balbuena, K.E. Gubbins, "Theoretical interpretation of adsorption behavior of simple fluids in slit pores," Langmuir 9 (1993) 1801-1814, doi: 10.1021/la00031a031.

[52] M. Thommes, "Physical adsorption characterization of nanoporous materials," Chem. Ing. Tech. 82 (2010) 1059-1073, doi: 10.1002/cite.201000064.

[53] J. Ke, X. Li, Q. Zhao, B. Liu, S. Liu, S. Wang, "Upconversion carbon quantum dots as a visible light-responsive component for efficient enhancement of photocatalytic performance," J. Colloid Interface Sci. 496 (2017) 425-433, doi: 10.1016/j.jcis.2017.01.121.

[54] S. Sun, J. Ding, J. Bao, C. Gao, Z. Qi, X. Yang, B. He, and C. Li, "Photocatalytic degradation of gaseous toluene on Fe-TiO_2 under visible light irradiation: a study on the structure, activity and deactivation mechanism," Appl. Surf. Sci. 258 (2012) 5031-5037, doi: 10.1016/j.apsusc.2012.01.075.

[55] A. Qu, H. Xie, X. Xu, Y. Zhang, S. Wen, and Y. Cui, "High quantum yield graphene quantum dots decorated TiO_2 nanotubes for enhancing photocatalytic activity," Appl. Surf. Sci. 375 (2016) 230-241, doi: 10.1016/j.apsusc.2016.03.077.

[56] G. Rajender, J. Kumar, P. Giri, "Interfacial charge transfer in oxygen-deficient TiO_2-graphene quantum dot hybrid and its influence on the enhanced visible-light photocatalysis," Appl. Catal., B 224 (2018) 960-972, doi: 10.1016/j.apcatb.2017.11.042.

[57] X. Chen, L. Liu, F. Huang, "Black titanium dioxide (TiO_2) nanomaterials," Chem. Soc. Rev. 44 (2015) 1861-1885, doi: 10.1039/C4CS00330F.

[58] Q. Zhang, P. Chen, M. Zhuo, F. Wang, Y. Su, T. Chen, K. Yao, Z.Cai, W. Lv, and G.Liu, "Degradation of indometacin by simulated sunlight activated CDs-loaded $BiPO_4$ photocatalyst: Roles of oxidative species," Appl. Catal., B 221 (2018) 129-139, doi: 10.1016/j.apcatb.2017.09.008.

[59] L. Xu, X. Bai, L. Guo, S. Yang, P. Jin, L. Yang, "Facial fabrication of carbon quantum dots (CDs)-modified N-TiO_2-x nanocomposite for the efficient photoreduction of Cr (VI) under visible light," Chem. Eng. J. 357 (2019) 473-486, doi: 10.1016/j.cej.2018.09.172.

[60] D. Qu, J. Liu, X. Miao, M. Han, H. Zhang, Z. Cui, S.Sun, Z. Kang, H. Fan, Z. Sun, "Peering into water splitting mechanism of g-C_3N_4-carbon dots metal-free photocatalyst," Appl. Catal., B 227 (2018) 418-424, doi: 10.1016/j.apcatb.2018.01.030.

[61] S. Morales-Torres, L. M. Pastrana-Martínez, J. L. Figueiredo, J. L. Faria, A. M. Silva, "Graphene oxide-P25 photocatalysts for degradation of diphenhydramine pharmaceutical and methyl orange dye," Appl. Surf. Sci. 275 (2013) 361-368, doi: 10.1016/j.apsusc.2012.11.157.

[62] C. Shen, L. Wang, A. Zhou, B. Wang, X. Wang, W. Lian, Q. Hu, G. Qin, and X. Liu, "Synthesis and electrochemical properties of two-dimensional RGO/Ti_3C_2Tx nanocomposites," Nanomaterials 8 (2018) 80, doi: 10.3390/nano8020080.

[63] H. Yu, Y. Zhao, C. Zhou, L. Shang, Y. Peng, Y. Cao, L.Wu, C. Tang, and T. Zhang, "Carbon quantum dots/TiO_2 composites for efficient photocatalytic hydrogen evolution," J. Mater. Chem. A 2 (2014) 3344-3351, doi: 10.1039/C3TA14108J.

[64] J. Zhu, Y. Tang, C. Yang, F. Wang, M. Cao, "Composites of TiO_2 nanoparticles deposited on Ti_3C_2 MXene nanosheets with enhanced electrochemical performance," J. Electrochem. Soc. 163 (2016) 785-A791, doi: 10.1149/2.0981605jes.

[65] C. Wang, K. Yang, X. Wei, S. Ding, F. Tian, F. Li, "One-pot solvothermal synthesis of carbon dots/Ag nanoparticles/TiO_2 nanocomposites with enhanced photocatalytic performance," Ceram. Int. 44 (2018) 22481-22488, doi: 10.1016/j.ceramint.2018.09.017.

[66] B. J. Morgan, G. W. Watson, "Intrinsic n-type defect formation in TiO_2: a comparison of rutile and anatase from GGA+ U calculations," J. Phys. Chem. C 114 (2010) 2321-2328, doi: 10.1021/jp9088047.

[67] J. Wang, and B. Renbi, "Formic acid enhanced effective degradation of methyl orange dye in aqueous solutions under UV–vis irradiation." Water Res. X, 101 (2016) 103-113, doi: 10.1016/j.watres.2016.04.044

[68] T. Kumar, and S. K. Ashok Kumar, "Visible-light-induced degradation of rhodamine B by nanosized Ag $_2$ S-ZnS loaded on cellulose." Photochem. Photobiol. Sci, 18 (2019) 148-154, doi: 10.1039/c8pp00330k

[69] A. Ullah, AKM Kibria, M. Akter, M. N. I. Khan, A. R. M. Tareq, and H. Firoz. Shakhawat , "Oxidative degradation of methylene blue using Mn 3 O 4 nanoparticles Water Conserv Sci Eng, 1 (2017) 249-256, doi: 10.1007/s41101-017-0017-3.

[70] X Ruibing, M Su, Y Liu, Z Chen, C Ji, M Yang, X Chang, and D Chen. "Comparative study on the removal of different-type organic pollutants on hierarchical tetragonal bismutite microspheres: adsorption, degradation and mechanism." J. Cleaner Prod 242 (2020),118366, doi: 10.1016/j.jclepro.2019.118366

[71] G. Salehi, R. Abazari, A. R. Mahjoub, "Visible-light-induced graphitic–C_3N_4@ nickel–aluminum layered double hydroxide nanocomposites with enhanced photocatalytic activity for removal of dyes in water," J. Inorg. Chem. 57 (2018) 8681-8691, doi: 10.1021/acs.inorgchem.8b01636.

[72] J. Zhang, Q. Liu, H. He, F. Shi, G. Huang, B. Xing, J. Jia, and C. Zhang, "Coal tar pitch as natural carbon quantum dots decorated on TiO_2 for visible-light photodegradation of rhodamine B," Carbon 152 (2019) 284-294, doi: 10.1016/j.carbon.2019.06.034.

[73] C. M. Magdalene, K. Kanimozhi, M. Arularasu, G. Ramalingam, K. Kaviyarasu, "Self-cleaning mechanism of synthesized SnO_2/TiO_2 nanostructure for photocatalytic activity application for wastewater treatment," Surf. Interfaces 17 (2019) 100346, doi: 10.1016/j.surfin.2019.100346.

[74] X. Miao, Z. Ji, J. Wu, X. Shen, J. Wang, L. Kong, M. Liu, and C. Song, "g-C_3N_4/AgBr nanocomposite decorated with carbon dots as a highly efficient visible-light-driven photocatalyst," J. Colloid Interface Sci. 502 (2017) 24-32, doi: 10.1016/j.jcis.2017.04.087.

[75] J.-F. Li, C.-Y. Zhong, J.-R. Huang, Y. Chen, Z. Wang, Z.-Q. Liu, "Carbon dots decorated three-dimensionally ordered macroporous bismuth-doped titanium dioxide with efficient charge separation for high-performance photocatalysis," J. Colloid Interface Sci. 553 (2019) 758-767, doi: 10.1016/j.jcis.2019.06.077.

[76] J. Zhang, M. Kuang, J. Wang, R. Liu, S. Xie, Z. Ji, "Fabrication of carbon quantum dots/TiO_2/Fe_2O_3 composites and enhancement of photocatalytic activity under visible light," Chem. Phys. Lett. 730 (2019) 391-398, doi: 10.1016/j.cplett.2019.06.011.

[77] N. C. Martins, J. Ângelo, A. V. Girão, T. Trindade, L. Andrade, and A. Mendes, "N-doped carbon quantum dots/TiO_2 composite with improved photocatalytic activity," Appl. Catal., B 193 (2016) 67-74, doi: 10.1016/j.apcatb.2016.04.016.

[78] Z. Chen, Y. Li, M. Guo, F. Xu, P. Wang, Y. Du, and P.Na, "One-pot synthesis of Mn-doped TiO_2 grown on graphene and the mechanism for removal of Cr (VI) and Cr (III)," J. Hazard. Mater. 310 (2016) 188-198, doi: 10.1016/j.jhazmat.2016.02.034.

[79] S. Bian, C. Zhou, P. Li, J. Liu, X. Dong, F. Xi, "Graphene quantum dots decorated titania nanosheets heterojunction: Efficient charge separation and enhanced visible-light photocatalytic performance," ChemCatChem. 9 (2017) 3349-3357, doi: 10.1002/cctc.201601594.

[80] Y. Li, Y. Xue, J. Tian, X. Song, X. Zhang, X. Wang, and H. Cui, "Silver oxide decorated graphitic carbon nitride for the realization of photocatalytic degradation over the full solar spectrum: from UV to NIR region," Sol. Energy Mater. Sol. Cells 168 (2017) 100-111, doi: 10.1016/j.solmat.2017.04.031.

[81] A. Bayat, E. Saievar-Iranizad, "Vertically aligned rutile TiO_2 nanorods sensitized with sulfur and nitrogen co-doped graphene quantum dots for water splitting: an energy level study," J. Alloys Compd. 755 (2018) 192-198, doi: 10.1016/j.jallcom.2018.05.008.

[82] A. Bayat, E. Saievar-Iranizad, "Synthesis of green-photoluminescent single-layer graphene quantum dots: determination of HOMO and LUMO energy states," J. Lumin. 192 (2017) 180-183, doi: 10.1016/j.jlumin.2017.06.055.

Table 1: Surface analysis data of Carbonized-$mTiO_2$, CD2@C-$mTiO_2$, and CD6@C-$mTiO_2$

Sample	BET surface area (m^2/g)	Average pore diameter (nm)	Pore volume (cm^3/g)
Carbonized-$mTiO_2$	156	1.87	0.2384
CD2@C-$mTiO_2$	185	1.87	0.2299
CD6@ C-$mTiO_2$	194	2.4	0.2674

Table 2: Comparison of photocatalytic performance in this research with previously reported in the literature

Entry	photocatalyst	Dye	Time (min)	Degradation (%)	Reference
1	CD/Ag/TiO_2	MB	120	20	[64]
2	g-C_3N_4@NiAl-LDH	RhB	240	93	[70]
3	CTP/TiO_2	RhB	360	91.1	[71]
4	SnO_2/TiO_2	MG	75	96	[73]
5	g-C_3N_4/CDs/AgBr	RhB	40	96	[74]
6	CDs/Bi:TiO_2	RhB	40	96.4	[75]
7	CQD/TiO_2/Fe_2O_3	MB	180	86.5	[76]
		MB	35	91	This work
8	CDs@C-$mTiO_2$	RhB	35	92	This work
		MO	35	95	This work

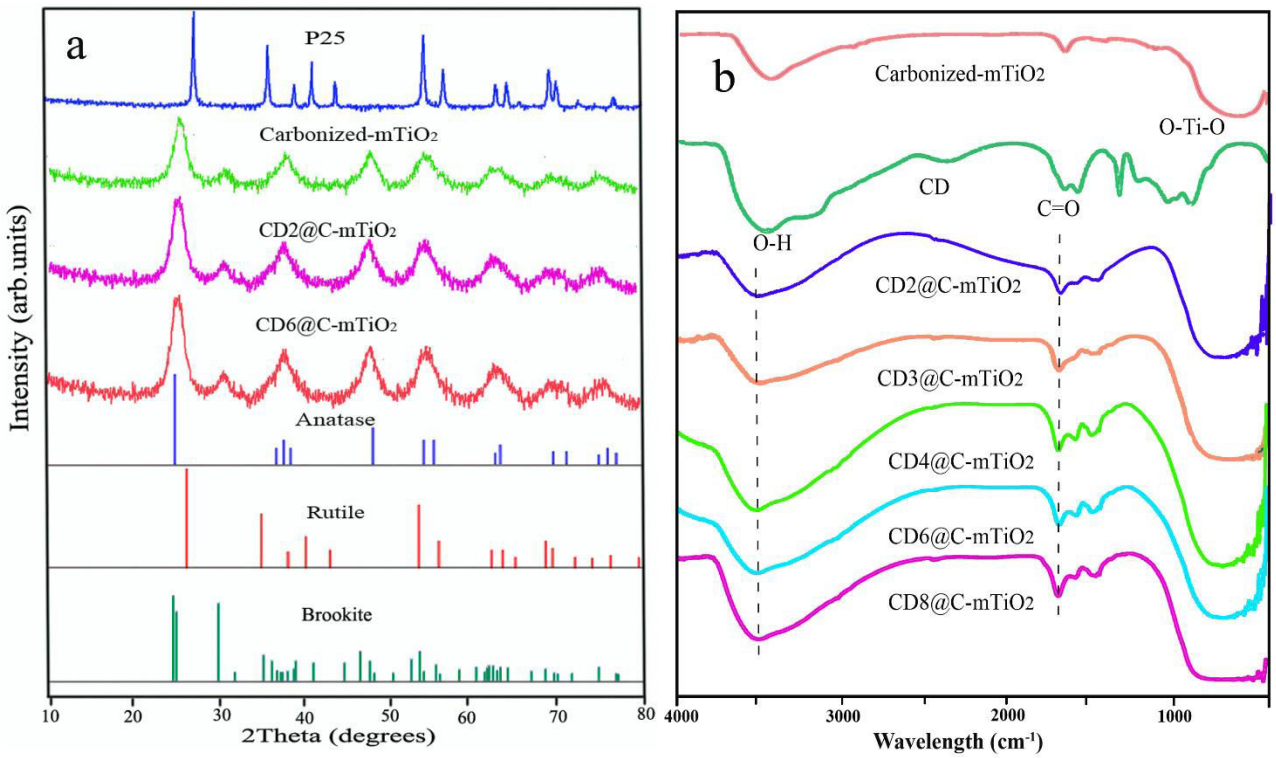

Figure 1. (a) XRD patterns and (b) FT-IR spectra of prepared samples.

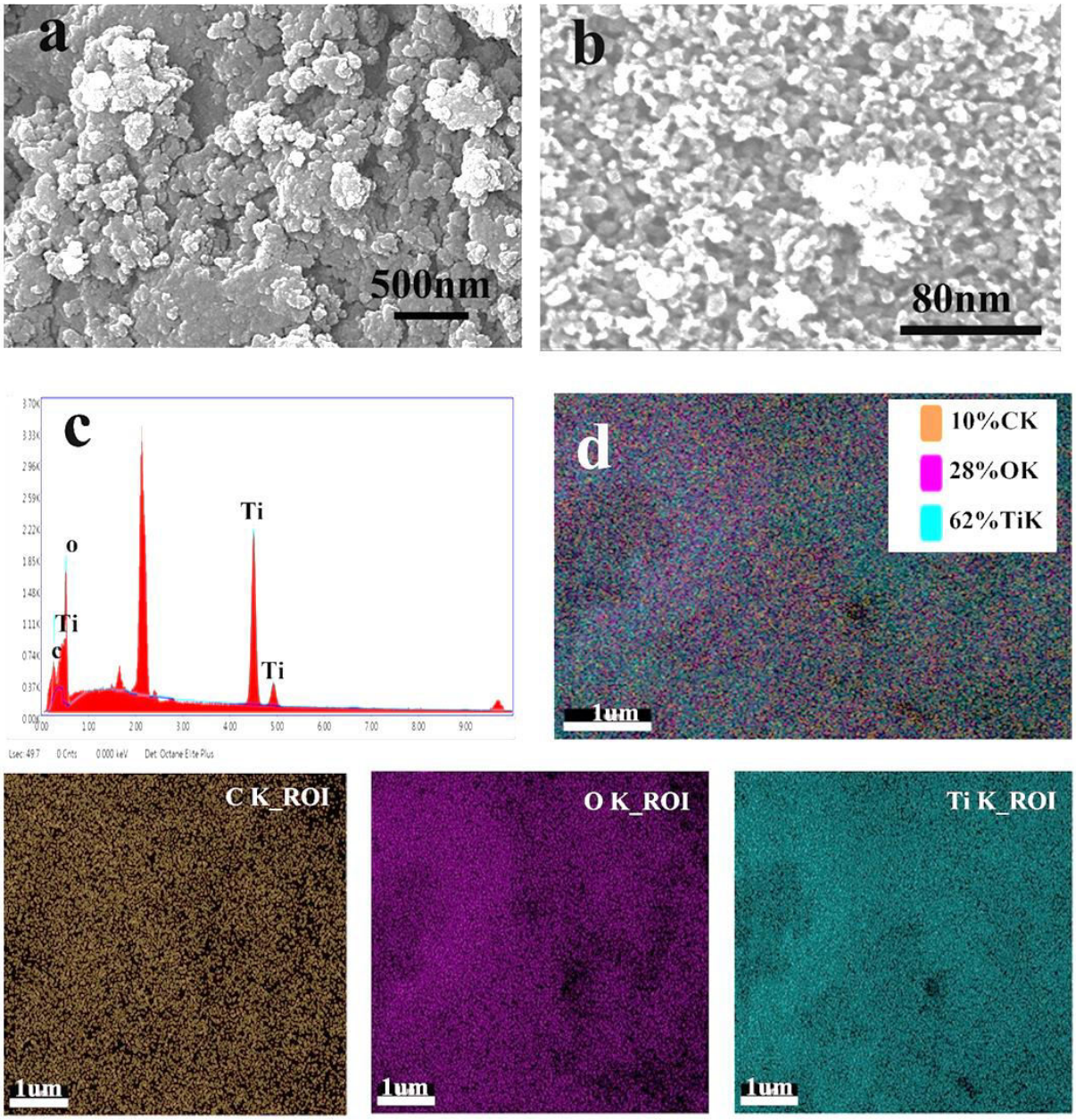

Figure 2. (a) FE-SEM, (b) STEM images, (c) EDX spectrum, and (d) elemental mapping image of CD6@C-mTiO_2.

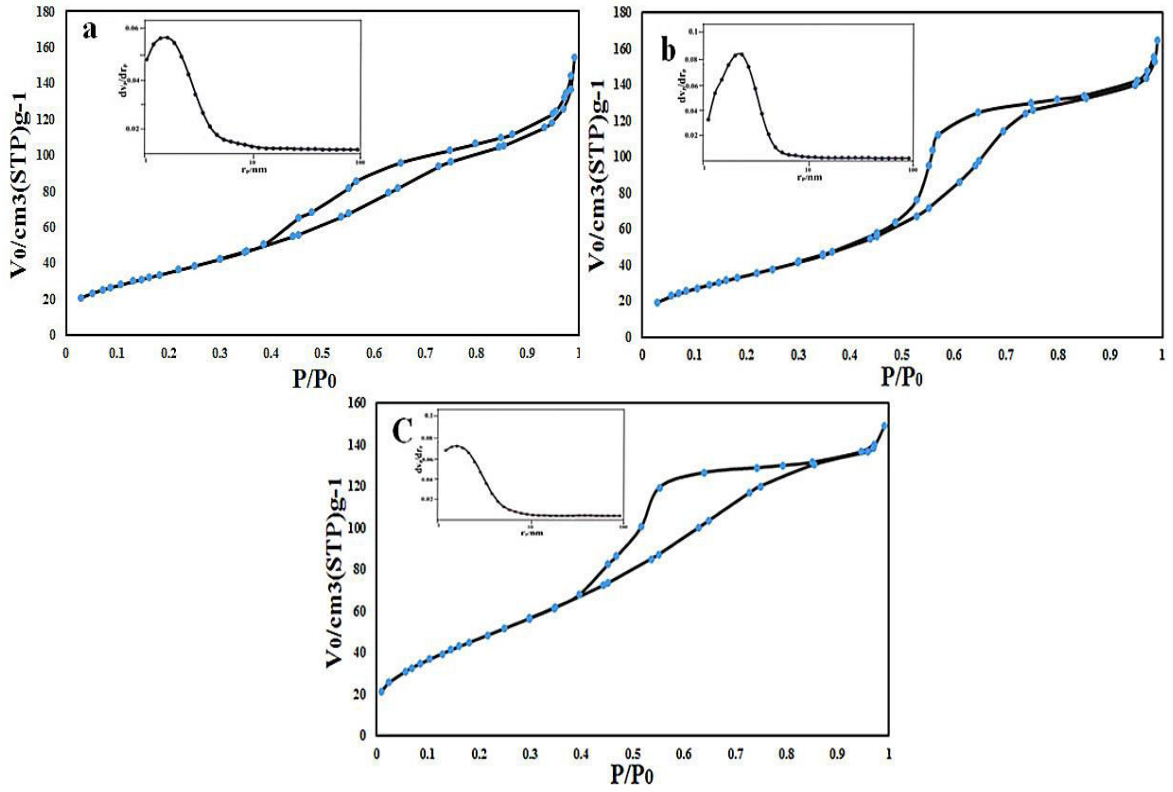

Figure 3. N_2 adsorption-desorption isotherms and BJH pore size distribution of samples (a) Carbonized-mTiO_2, (b) CD2@C-mTiO_2, (c) CD6@C-mTiO_2.

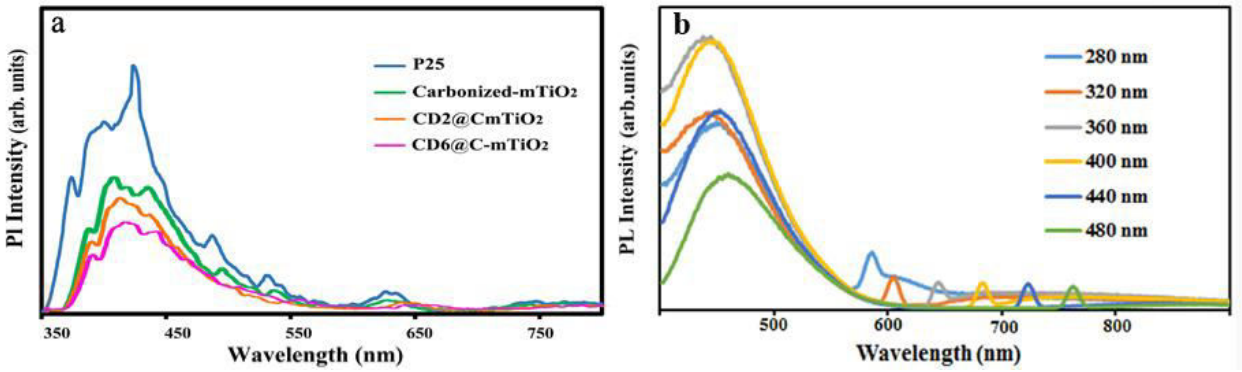

Figure 4. (a) Solid state photoluminescence (PL) spectra of the samples under excitation of 320 nm, (b) Photoluminescence spectra of carbon dots in polyethylene glycol solution measured upon excitation at different photon energies.

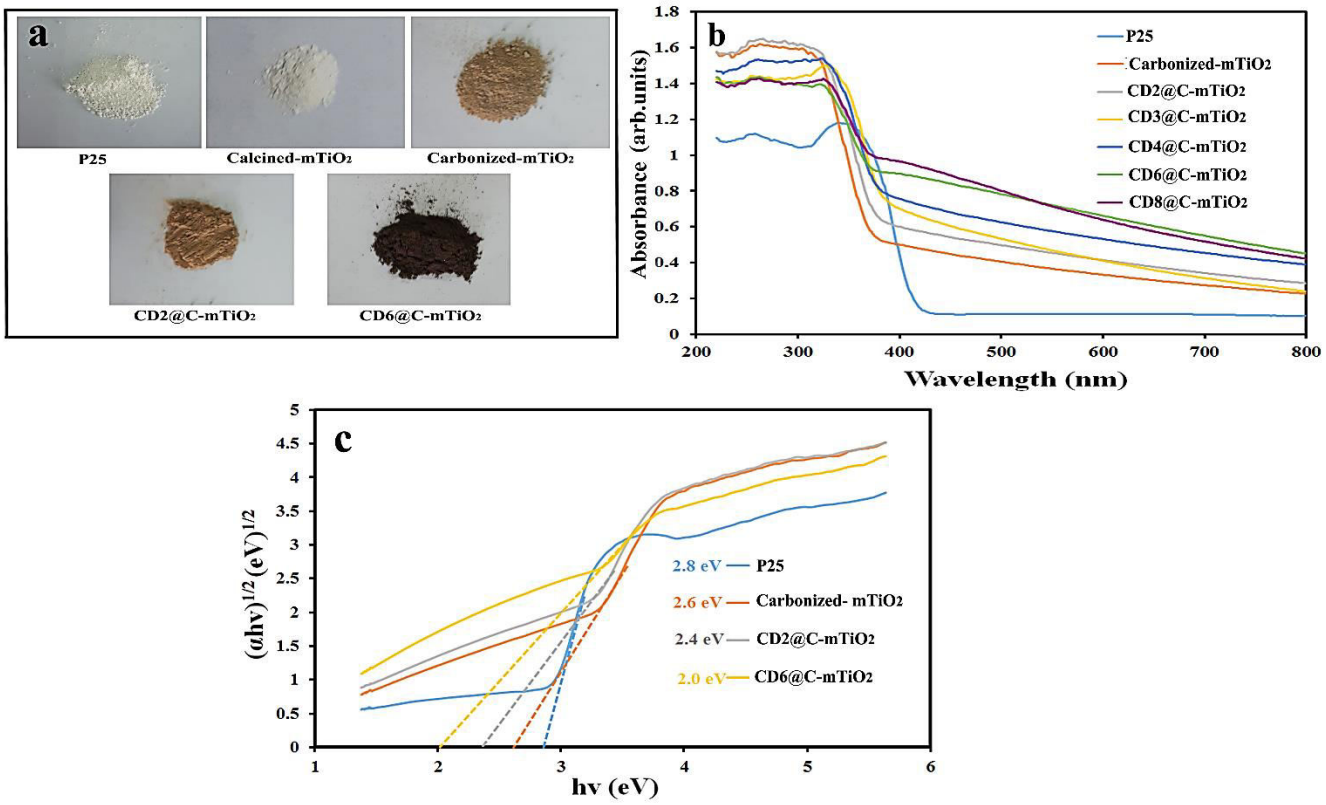

Figure 5. **(**a) Photographs of as-prepared photocatalysts, (b) UV-vis diffuse reflectance spectrum and (c) plots of $(\alpha h\nu)^{1/2}$ versus $h\nu$ of samples C-mTiO$_2$ and CDs@C-mTiO$_2$. (d) Photoluminescence spectra of CDs.

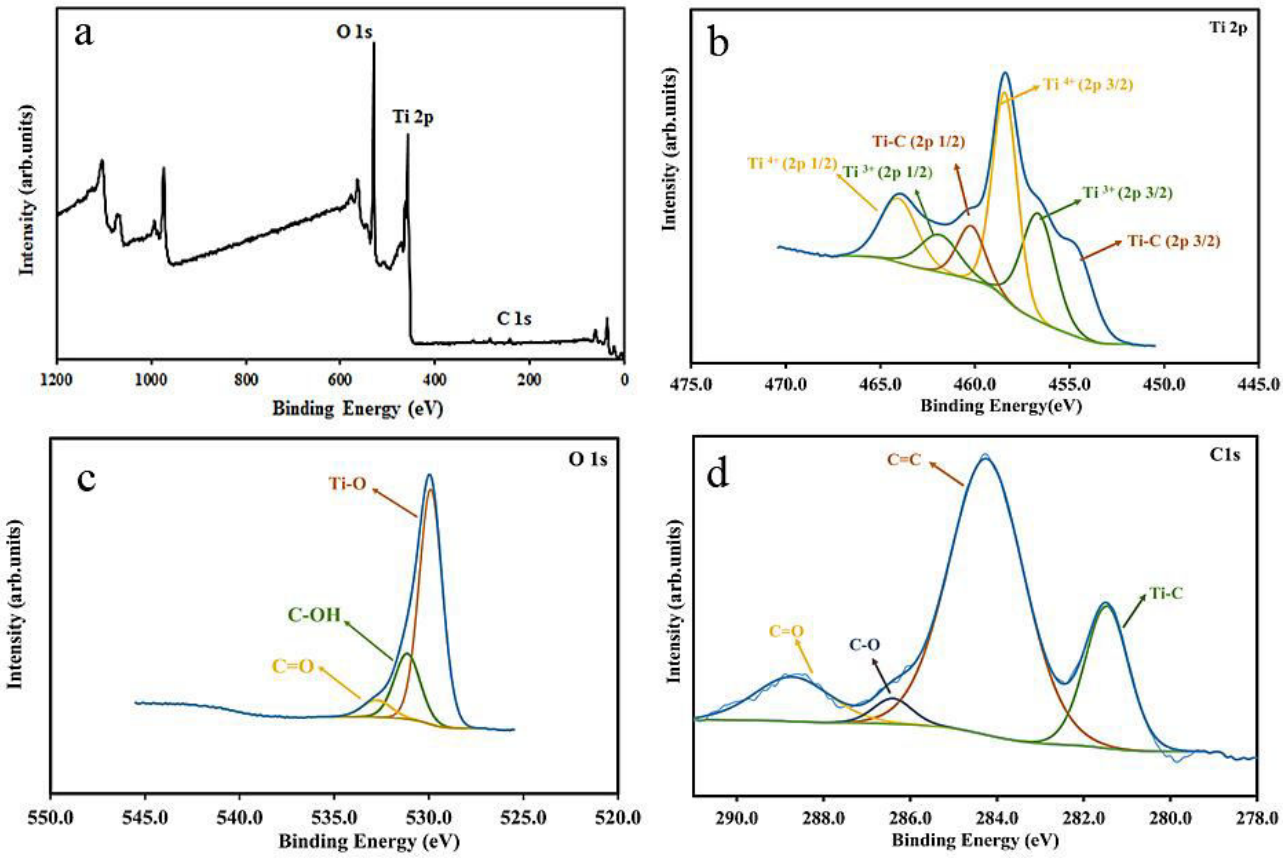

Figure 6. XPS spectra of sample CD6@C-mTiO_2. (a) Survey scan, and narrow scans of (b) Ti 2p, (c) C 1s, and (d) O 1s spectra.

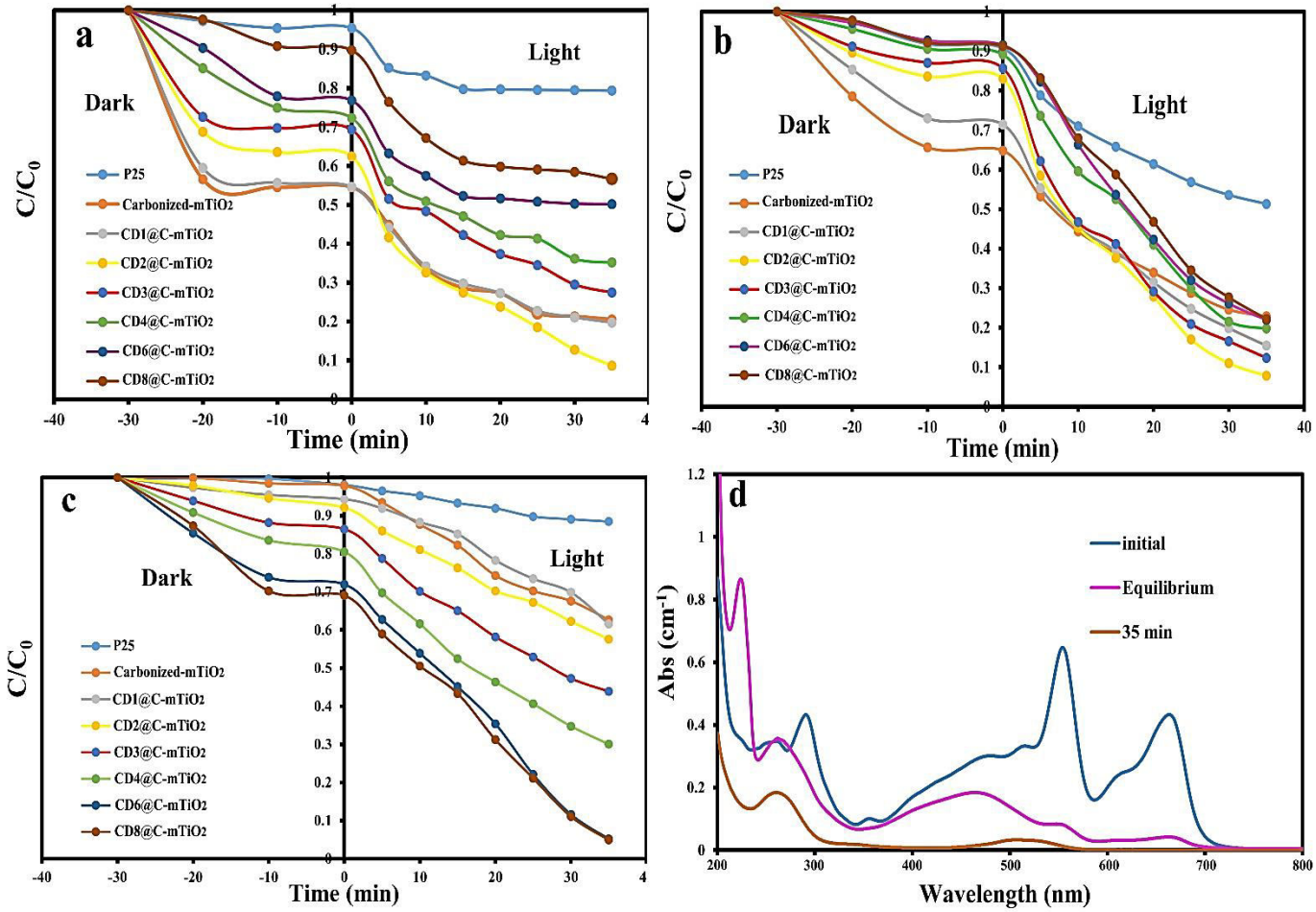

Figure 7. Photocatalytic degradation of (a) MB, (b) RhB and (c) MO in presence of different photocatalysts. (d) Photocatalytic degradation of mixed dyes by sample CD4@C-mTiO$_2$ under visible light.

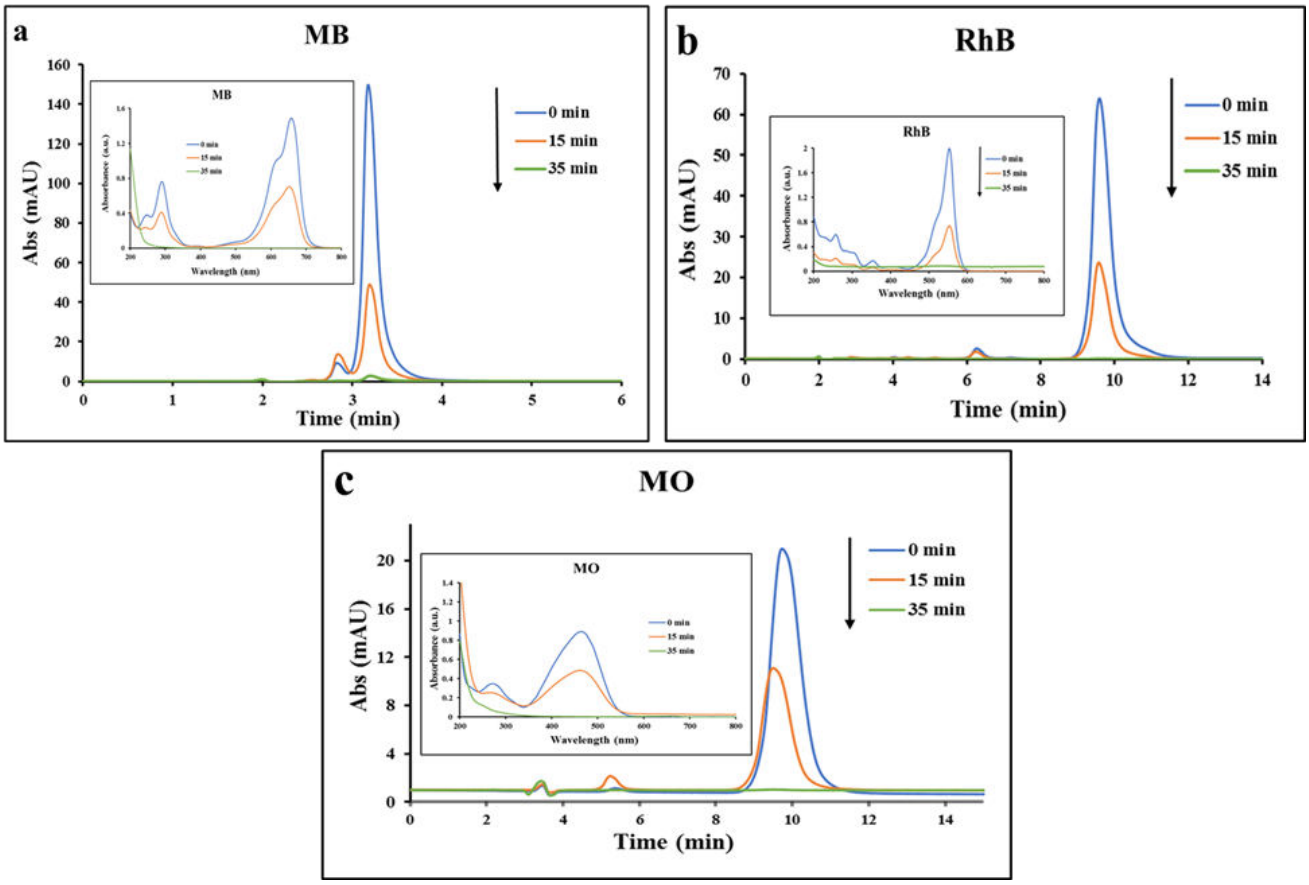

Figure 8. HPLC and UV-vis results of photocatalytic degradation of a) MB, b) RhB, and c) MO in presence of the best photocatalyst.

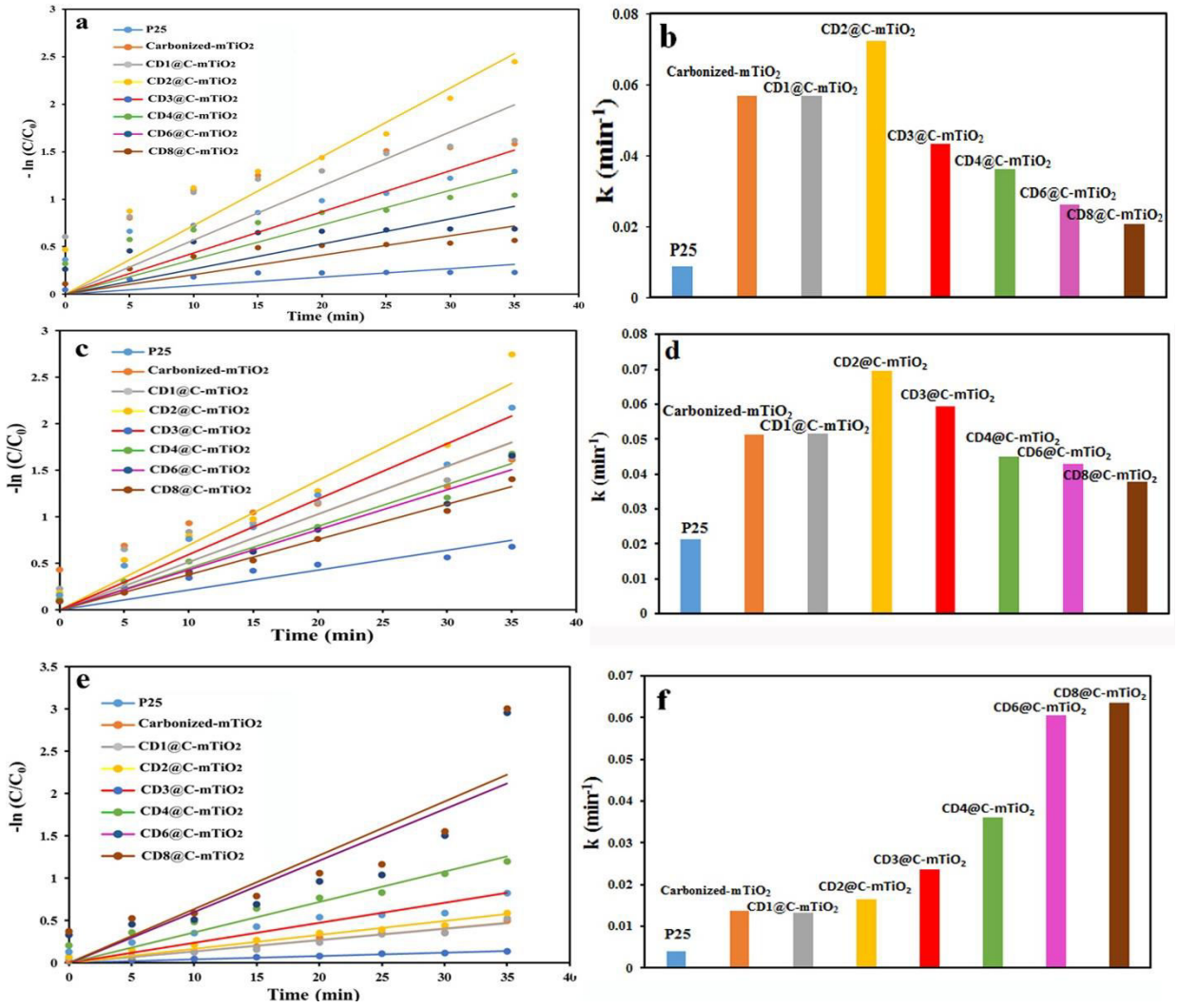

Figure 9. Linear fitting of the pseudo-first-order kinetic model of photocatalytic degradation of (a) MB, (c) RhB, and (e) MO. Degradation rate constants of (b) MB, (d) RhB, and (f) MO in presence of different photocatalysts.

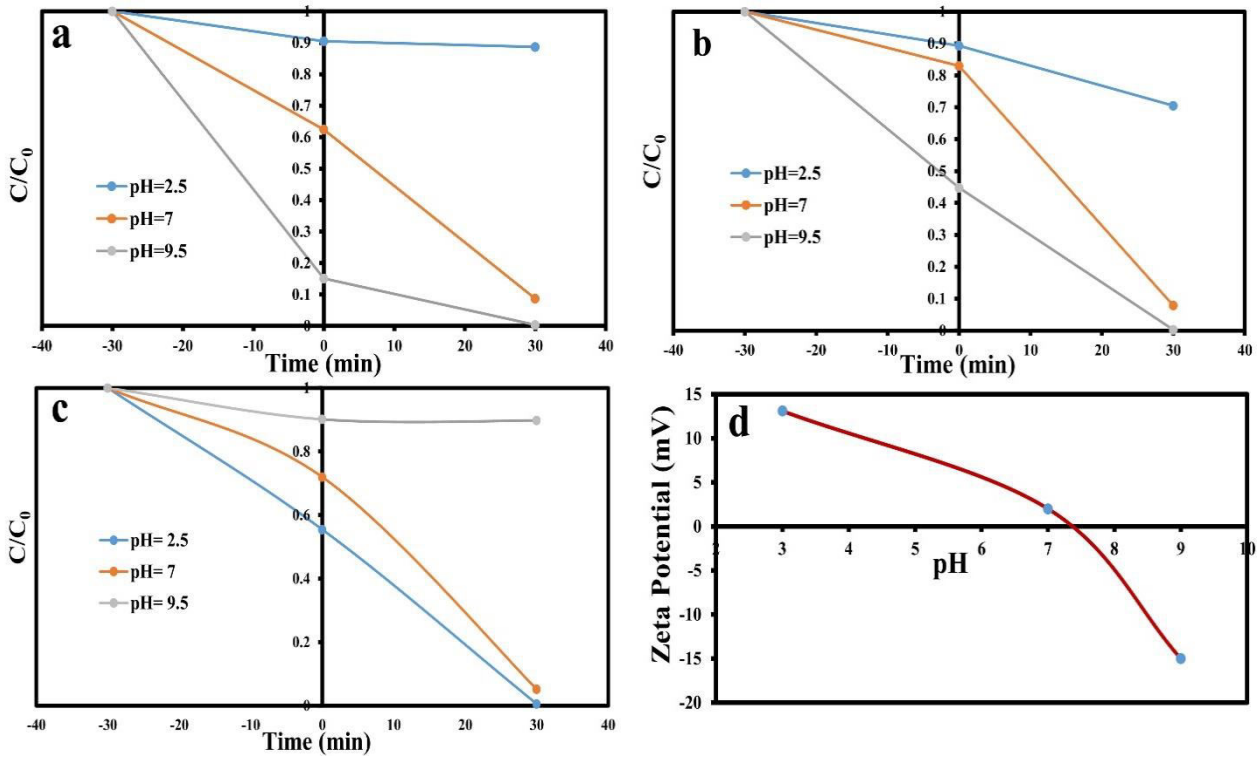

Figure 10. Effect of initial medium pH on degradation of (a) MB, (b) RhB, and (c) MO under visible light irradiation. (d)Zeta potential values of carbon dots at different pH.

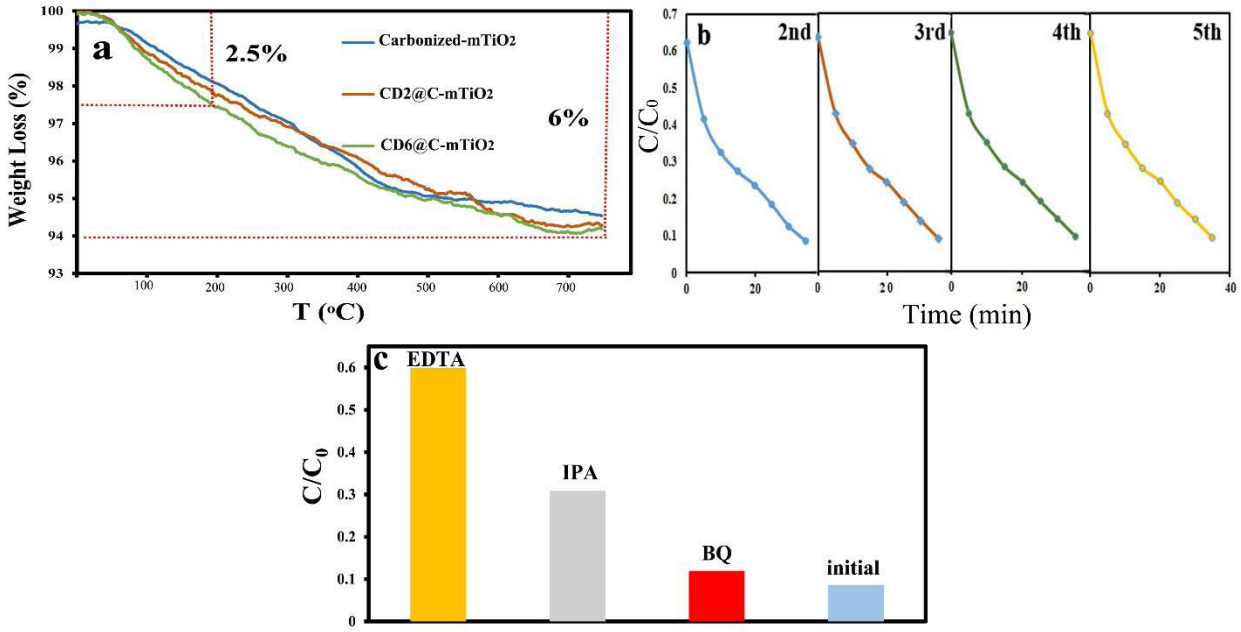

Figure 11. (a) TGA curve of samples Carbonized-mTiO$_2$, CD2@C-mTiO$_2$, and CD6@C-mTiO$_2$. (b) Photocatalytic performance during five subsequent cycles of degradation and (c) effect of different scavengers on the photocatalytic activity of CD2@C-mTiO$_2$ in degradation of MB in 35 min

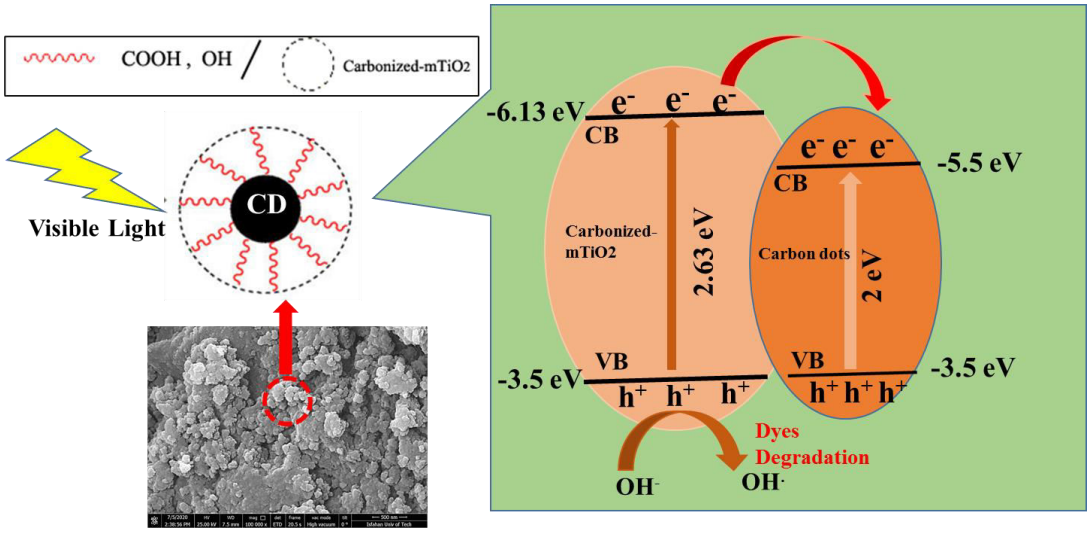

Figure 12. Schematic presentation of photogenerated charge transfer and free-radical generation in CD@C-mTiO$_2$ composites with a possible reaction mechanism during their photocatalytic performance.